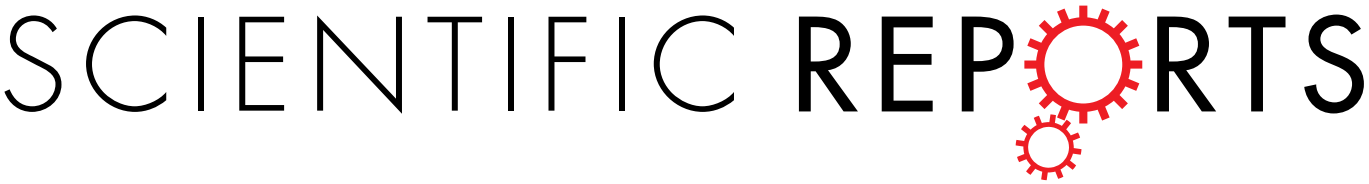

OPEN

Extremely high-performance visible light photodetector in the Sb_2SeTe_2 nanoflake

Received: 12 January 2017
Accepted: 23 February 2017
Published: 28 March 2017

Shiu-Ming Huang[1], Shih-Jhe Huang[1], You-Jhih Yan[2], Shih-Hsun Yu[2], Mitch Chou[2,3], Hung-Wei Yang[4], Yu-Shin Chang[4] & Ruei-San Chen[4]

The photocurrent was performed in the Sb_2SeTe_2 topological insulator at a wavelength of 532 nm. It exhibits extremely high performance that the responsivity and the photoconductive gain reach 2293 AW^{-1} and 5344 at 1 V. This high photoresponse is orders of magnitude higher than most reported values in topological insulators and two-dimensional transitional metal dichalcogenides. This finding suggests that the Sb_2SeTe_2 nanoflake has great potential for future optoelectronic device applications.

A system that generates a high photocurrent in response to light may be used as a photosensor. The light penetration distance is very short; thus, the photoresponse properties are dominated by the carriers near the material surface. A material with a relatively high surface carrier dominance can be expected to perform as a relatively efficient photodetector. To optimize the photoresponse, various types of nanostructured materials, with high surface-to-volume ratios and high levels of photoresponse, were investigated[1–6]. Recently, two-dimensional materials such as graphene[7,8], graphene-based heterostructures[1–4], and two-dimensional transitional metal dichalcogenides (TMDs) have attracted noteworthy attention[9–16]. These two-dimensional materials demonstrate excellent photoelectrical performance because they have high surface-to-volume ratios and abundant surface carriers.

Three-dimensional topological insulators are promising materials because they offer insulating bulk states and a gapless conducting surface state. These insulators have a surface state that is topologically protected by a time reversal symmetry, which is induced by a strong spin-orbit interaction. This remarkable surface state has garnered intensive theoretical and experimental attention and had been a recent research topic[17,18]. The linear dispersions in the surface state and the extremely high carrier mobility levels make these insulators promising candidates for optical electrical devices[19,20]. The photoelectrical characteristics of the Bi-based topological insulators have been investigated and have revealed promising responses[21,22]. It is reported that the Bi_2Te_3 topological insulator based heterostructures[1,23,24] and PLD-grown Bi films[25] reveal ultrahigh responsivity in wide wave range. Recently, it was reported that Sb_2Te_3 thin films offer higher photoelectrical responses than that in Bi-based topological insulators[26].

In this paper, we report on the photocurrent produced by a 532-nm wavelength in a Sb_2SeTe_2 topological insulator. The experimental results reveal extremely high performance; specifically, the responsivity and the photoconductive gain reached 2293 AW^{-1} and 5344 at a bias of 1 V. These observations are orders of magnitude higher than most reported values in other topological insulators and two-dimensional TMDs, which suggests that Sb_2SeTe_2 nanoflakes have great potential for future optoelectronic device applications.

Experimental method

Single crystals of Sb_2SeTe_2 were grown by a homemade resistance-heated floating zone furnace (RHFZ). The starting raw materials of Sb_2SeTe_2 were mixed according to the stoichiometric ratio. At first, the stoichiometric mixtures of high purity elements Sb (99.995%), Se (99.995%) and Te (99.995%) were melted at temperatures of 700 ~800 °C for 20 h, and then slowly cooled to room temperature in an evacuated quartz glass tube. The resulting material was used as a feeding rod for the following RHFZ experiment. After growth, the crystals were then furnace cooled to room temperature. The as-grown crystals were cleaved along the basal plane, producing a silvery

[1]Department of Physics, National Sun Yat-Sen University, Kaohsiung 80424, Taiwan. [2]Department of Materials and Optoelectronic Science, National Sun Yat-Sen University, Kaohsiung 80424, Taiwan. [3]Taiwan Consortium of Emergent Crystalline Materials, TCECM, National Sun Yat-Sen University, Kaohsiung 80424, Taiwan. [4]Graduate Institute of Applied Science and Technology, National Taiwan University of Science and Technology, Taipei 10607, Taiwan. Correspondence and requests for materials should be addressed to S.-M.H. (email: smhuang@mail.nsysu.edu.tw)

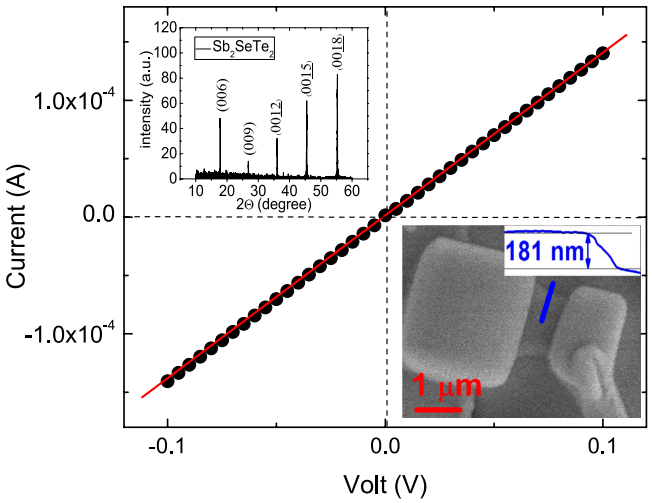

Figure 1. Left-top inset shows the XRD of the Sb_2SeTe_2. The sharp peaks indicate the high crystallinity of the Sb_2SeTe_2 crystal. The right-bottom inset shows a SEM picture of the Sb_2SeTe_2 nanoflake. The red line is the scale bar of SEM. The blue curve is the AFM thickness profile and the sample thickness is 181 nm. Two Pt contacts were deposited on the nanoflake to measure the photocurrent. The linear current-voltage curve indicates the ohmic contact between the Pt electrodes and the Sb_2SeTe_2 nanoflake.

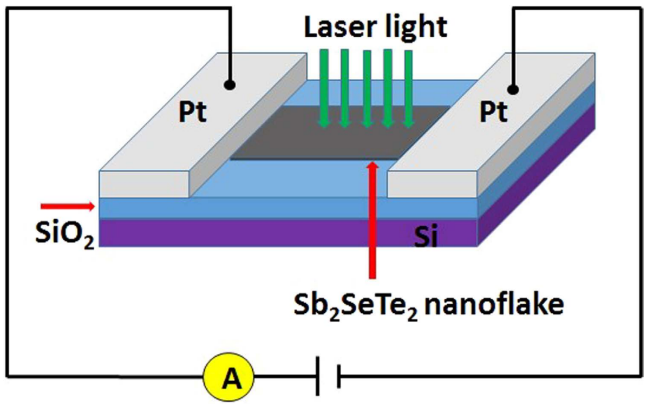

Figure 2. Schematic of the Sb_2SeTe_2 nanoflake device illustrating the photoelectrical measurement setup and the light that illuminated it. The wavelength of the light was 532 nm.

shining mirror-like surface, and then prepared for the further experiments. The Raman[27], EDS and XPS[28] spectrum support that the crystal is Sb_2SeTe_2.

The Sb_2SeTe_2 nanoflakes were obtained by exfoliating bulk crystals using dicing tape and were then dispersed on the insulating SiO_2 (300 nm)/*n*-Si templates with pre-patterned Ti/Au circuits. Two platinum (Pt) metal contacts were subsequently deposited on the selected Sb_2SeTe_2 nanoflakes using focused-ion beam (FIB) technique (shown in the right-bottom inset of Fig. 1). The thickness of a nanoflake is determined by the atomic force microscopy; here, the nanoflake was 181-nm thick, 708-nm long, and 1667-nm wide. The current-voltage characteristic reveals a linear dependence that indicates the ohmic contacts in the sample; the conductivity was approximately 33.7 *S*/*cm*. The left-top inset within Fig. 1 shows the X-ray diffraction of the Sb_2SeTe_2; the sharp peaks indicate that the Sb_2SeTe_2 crystal has high crystallinity. Our previous works show that the physical parameters extracted from XPS, Raman spectrum, ARPES and the quantum SdH oscillation are consistent. That supports the Sb_2SeTe_2 crystal reveals high quality and uniformity. Figure 2 presents the schematic of the Sb_2SeTe_2 nanoflake device, illustrating the photoelectrical measurement setup and the light that illuminated it. The wavelength of the illuminating light was 532 nm.

Results and Discussion

The inset of the Fig. 3 shows that the measured current of our Sb_2SeTe_2 nanoflake under light illumination with light power that ranges from 1 to 50 mW that is corresponding to the power intensity of 40 to 2000 Wm^{-2}. It clearly indicates that the current increases with increasing light power. The overall response time is approximately 10 s; which is shorter than the reported values of Sb_2Te_3 films[26], but longer then the values of Bi-based topological

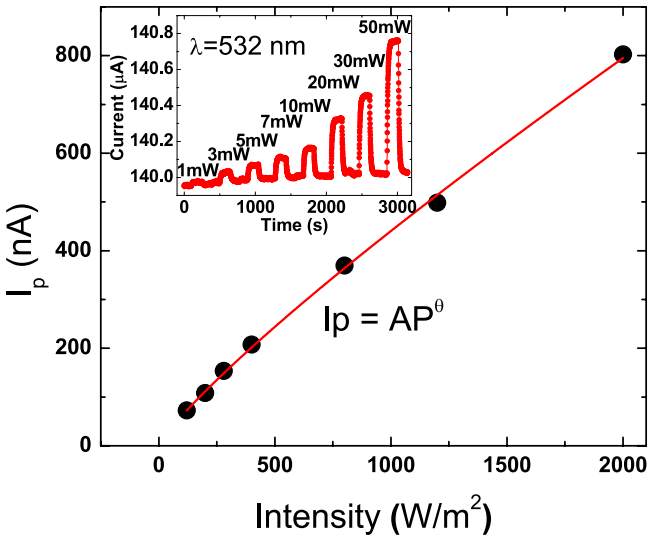

Figure 3. Left-top inset depicts the photocurrents produced by illumination at different power levels. The measured photocurrent is a function of light power intensity, and can be accurately described by a simple power law relation.

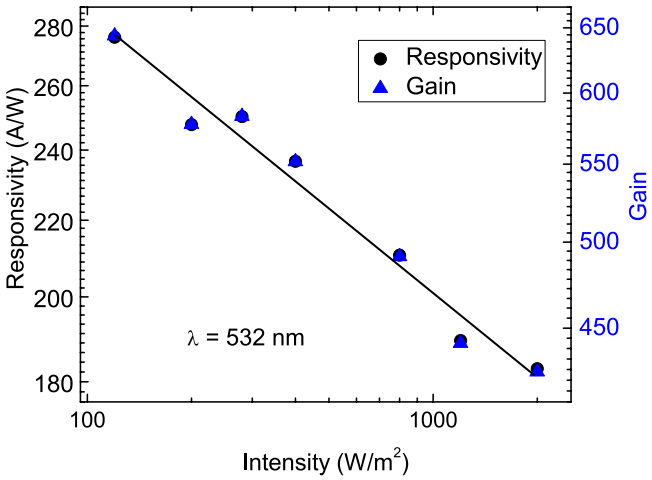

Figure 4. Responsivity and photoconductive gain as functions of the light power intensity at a wavelength of 532 nm. Both responsivity and photoconductive gain increase as the light power intensity decreases.

insulators[21,22]. Here the photocurrent is presented as a function of the power intensity at bias of 0.1 V (Fig. 3). For quantitative analysis, the relationship between the photocurrent and the light intensity can be fitted to the simple power law relation, $I_p = AP^\theta$, where the A is a constant for the wavelength of the illuminating light, P is the power intensity of the light that illuminates the device, and θ is a constant related the photosensitivity of the device. As Fig. 3 reveals, the experimental data agrees with the power law relation and the fitting result gives a θ of 0.85.

To quantitatively determine the performance of the Sb_2SeTe_2 nanoflake under illumination, responsivity, R, and the photoconductive gain, G, are calculated through the following equations;

$$R = \frac{I_P}{PS}, \tag{1}$$

$$G = \frac{hcR}{\eta e\lambda} = \frac{1240R}{\eta\lambda}, \tag{2}$$

where I_P, P, S, h, c, e, η and λ are the photocurrent, the light intensity, the effective area, Planck's constant, the velocity of light, the charge of an electron, the quantum efficiency (for convenience, we assume $\eta = 1$) and the wavelength, respectively. The G for a wavelength is proportional to the R at the same wavelength. Figure 4 depicts R and G as functions of the light intensity at a constant bias of 0.1 V, and reveals that the R and G decrease as the power intensity increases. Specifically, the R and G are 276 AW^{-1} and 643 at a power intensity of 120 Wm^{-2}.

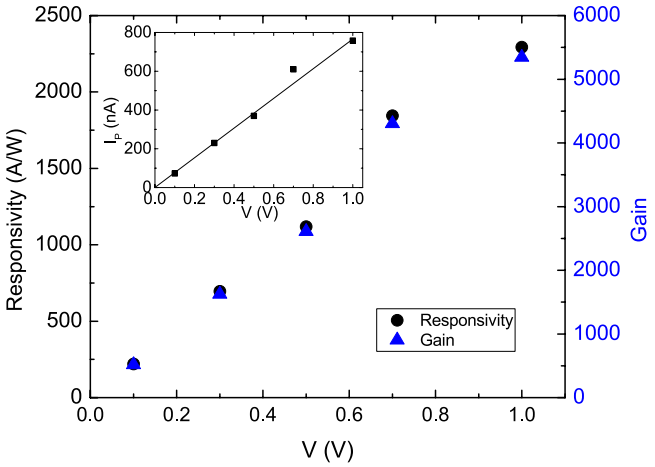

Figure 5. Left-top inset shows the linear relation of a photocurrent to the applied bias at a wavelength of 532 nm and a power intensity of 280 W/m^2. The main figure shows the responsivity and the photoconductive gain as functions of the applied bias at a wavelength of 532 nm and the power intensity of 280 W/m^2.

The photocurrent is strongly related to the applied bias. To comprehensively investigate the intrinsic optoelectronic characteristics in the Sb_2SeTe_2 nanoflake, an experiment on bias-dependent photocurrents was performed. As shown in the inset of the Fig. 5, the photocurrent was linearly related to the applied bias; specifically, the observed photocurrent was approximately 0.8 μA at 1 V and a light power intensity of 280 Wm^{-2}. This linear bias-dependent increment of the photocurrent can be attributed to the increment drift velocity and the reduced carrier transit time caused by applied bias. Expressed as $T = l^2/\mu V_{sd}$, T is the carrier transit time, l is the device length, μ is the carrier mobility, and V_{sd} is the applied bias. This indicates a system with higher carrier mobility; and, a higher bias might decrease the carrier transit time, and produce a higher photocurrent. Figure 5 also indicates that the evaluated R and G are functions of bias, to which both linearly relate. At 1 V, The R and G reach 2293 AW^{-1} and 5344, respectively.

To qualitatively identify the optical performance of the Sb_2SeTe_2 nanoflake, the reported values were collected. Table 1 presents a list of the reported R and G values for topological insulators and two-dimensional TMDs, and clearly reveals that the R and G values for our Sb_2SeTe_2 are orders of magnitude higher than most the reported values in topological insulators and two-dimensional TMDs under similar conditions. That suggests that the Sb_2SeTe_2 has the potential to deliver extremely high-performance photocurrent-related applications.

Aside from the high quality of the crystalline sample and the large surface-to-volume ratio, several possible causes might lead to this extremely high photoresponse. First, the photoresponse is extremely sensitive to the condition of sample surface. In addition to the reduction of the effective response area, surface defects and oxidation reduce carrier mobility and life time. One prior study reported that adsorbed molecules on a surface reduce the carrier's life time; thus, the photoresponse of a material in a vacuum is higher than the photoresponse of the same material in the air[29]. Our previous work revealed that the surface state carrier transport characteristics in our Sb_2SeTe_2 topological insulator can tolerant surface oxidation and molecules adsorbed on the sample's surface; such molecules might come from unavoidable pollution during the fabrication process or from sample transference[28]. Therefore, less effective defective materials might impair the surface electron transport properties of our Sb_2SeTe_2 sheet, and the proposed nanoflake might be very effectively by comparison. Second, in addition to the artificial and extrinsic factors, R and G values are directly related to carrier mobility. The reported R and G in MoS_2 and WSe_2 flakes were positively related to the field-effect carrier mobility[30]. The surface state carrier mobility of our Sb_2SeTe_2 topological insulator was approximately 55.5 $cm^2V^{-1}s^{-1}$ at room temperature[31]; that is one order larger than the previously reported value (4 $cm^2V^{-1}s$) for a single-layer MoS_2 flake[30]. Third, it is noteworthy that previous works have revealed that graphene-based heterostructure greatly enhances photoresponse because electron have high mobility in graphene and two-dimensional TMDs demonstrate enhanced adsorption ratios. The R and G values of our Sb_2SeTe_2 are orders of magnitude higher than most reported values in topological insulators and two-dimensional TMDs, and are only lower than the reported values in the nanowires[5,6,32]. and graphene-MoS_2 hybrid structure[1]. Theoretical calculation shows that the surface state Dirac point lies at the energy gap of the bulk state in Sb_2SeTe_2, and our previous work supported that the Fermi level is below the Dirac point. This energy band structure is similar to the graphene-MoS_2 hybrid structure and might lead to the observed high photoresponse.

Detectivity, that is an important figure-of-merit in evaluating the ability of a photodetector to detect weak signal, is another important indices used to characterize the performance of photodetectors[33]. The specific detectivity (D^*) is calculated through the relation:

$$D^* = \frac{RS^{1/2}}{(2qI_d)^{1/2}}, \tag{3}$$

material	wavelength (nm)	Bias (V)	Responsivity (AW^{-1})	Gain (EQE)	reference
Sb_2SeTe_2 nanoflake	532	1	2293	5344	This work
Sb_2SeTe_2 nanoflake	532	0.1	276	643	This work
Sb_2Te_3 film	980	0.01	0.26	0.33	ref. 26
Sb_2Te_3 film	980	0.1	2.31	2.93	ref. 26
Sb_2Te_3 film	980	1	21.7	27.4	ref. 26
Bi_2Se_3 nanowire	1064	0.1	207	241	ref. 21
Bi_2Se_3 nanowire	1064	0.15	300	350	ref. 21
Bi_2Te_3 polycrystal	1064	0.3	3×10^{-5}	3.85×10^{-5}	ref. 22
graphene – Bi_2Te_3	1550	1	0.22	0.17	ref. 34
graphene – Bi_2Te_3	980	1	10	11	ref. 34
graphene – Bi_2Te_3	532	1	36.7	85.8	ref. 34
Bi_2Se_3 nanosheet (exfoliated)	532	0.6	20.4×10^{-3}		ref. 35
Pristine Bi_2Se_3 bulk	532	0.6	2.45×10^{-3}		ref. 35
Heat-treated Bi_2Se_3 nanosheets	532	0.6	16.1×10^{-3}		ref. 35
Graphene	532	0.1	8.61		ref. 7
Graphene	1550	0.4	6×10^{-3}		ref. 8
GaSe	254	5	2.8	13.67	ref. 9
GaS	254	2	4.2	20.5	ref. 10
MoS_2	670	1	4.2×10^{-4}		ref. 11
MoS_2	532	5	~6		ref. 12
MoS_2	532	10	0.57	13.3	ref. 13
MoS_2	532	1	780	1840	ref. 14
MoS_2	633	1	120		ref. 15
MoS_2 nanoflake	532	1	30	103	ref. 29
MoS_2 nanoflake	561	8	880		ref. 30
MoS_2	655	5	4.1		ref. 36
APTES-doped MoS_2	655	5	56.5		ref. 36
OTS-doped MoS_2	655	5	0.36		ref. 36
WS_2	655	5	20		ref.36
APTES-doped WS_2	655	5	0.59		ref. 36
OTS-doped WS_2	655	5	36.4		ref. 36
WS_2 film	635	9	0.7	137%	ref.37
WSe_2 film	635	10	0.92	180%	ref.38
WSe_2 monolayer	650	2	1.8×10^5	3.5×10^5	ref. 39
$Mo_{0.5}W_{0.5}S_2$ polycrystal film	635	2.2	5.8	11.35%	ref. 40
$MoTe_2$	473	0.5	2560	6700	ref. 41
$HfSe_2$ multilayer	800	2	3961		ref. 42
In_2Se_3 nanosheet	300	5	395	1630	ref. 43
In_2Se_3 nanosheet	400	5	110	340	ref. 43
In_2Se_3 nanosheet	500	5	59	146	ref. 43
InSe layers	532	5	0.101	0.235	ref. 44
$NbSe_2$ nanoflake	532	0.1	2.3	300	ref. 45
$NbSe_2$ nanoflake	808	0.1	3.8	300	ref. 45

Table 1. List of the reported responsivity and gain values of photocurrents in topological insulators and two-dimensional transition metal dichalcogenides.

where R, S, q, and I_d are the responsivity, effective area of light illumination, electronic charge, and dark current. By using the experimental data, the detectivity is determined to be 4.5×10^8 Jones.

Conclusion

A photocurrent experiment was performed in a Sb_2SeTe_2 topological insulator nanoflake at a wavelength of 532 nm. It exhibited extremely high performance; the responsivity and the photoconductive gain were 2293 AW^{-1} and 5344 at 1 V, respectively. This high photoresponse was orders of magnitude higher than most reported values in topological insulators and two-dimensional TMDs. This finding suggests that the Sb_2SeTe_2 nanoflake has remarkable potential for future optoelectronic device applications.

References

1. K. Roy *et al.* Graphene-MoS_2 hybrid structures for multifunctional photoresponsive memory devices. *Nat. Nanotech* **8,** 826–830 (2013).
2. W. J. Zhang *et al.* Ultrahigh-Gain Photodetectors Based on Atomically Thin Graphene-MoS_2 Heterostructures. *Sci. Rep.* **4,** 3826–3833 (2014).
3. G. Konstantatos *et al.* Hybrid graphene-quantum dot phototransistors with ultrahigh gain. *Nat. Nanotech* **7,** 363–368 (2012).
4. C. Chen *et al.* Highly responsive MoS_2 photodetectors enhanced by graphene quantum dots. *Sci. Rep*. **5,** 11830–11838 (2015).
5. C. Soci *et al.* ZnO Nanowire UV Photodetectors with High Internal Gain. *Nano Lett*. **7,** 1003–1009 (2007).
6. R. S. Chen *et al.* Photoconduction efficiencies of metal oxide semiconductor nanowires: The material's inherent properties. *Appl. Phys. Lett.* **103,** 223107–223111 (2013).
7. Y. Zhang, T. Liu, B. Meng, X. Li, G. Liang, X. Hu & Q. J. Wang. Broadband high photoresponse from pure monolayer graphene photodetector. *Nat. Communi*. **4,** 1811–1821 (2013).
8. T. Mueller, F. Xia & P. Avouris. Graphene photodetectors for high-speed optical communications. *Nat. Photonics* **4,** 297–301 (2010).
9. P. A. Hu *et al.* Synthesis of Few-Layer GaSe Nanosheets for High Performance Photodetectors. *ACS Nano* **6,** 5988–5994 (2012).
10. P. A. Hu *et al.* Highly Responsive Ultrathin GaS Nanosheet Photodetectors on Rigid and Flexible Substrates. *Nano Lett*. **13,** 1649–1654 (2013).
11. Z. Lin *et al.* Single-Layer MoS_2 Phototransistors. *ACS Nano* **6,** 74–80 (2012).
12. M. M. Furchi *et al.* Mechanisms of Photoconductivity in Atomically Thin MoS_2. *ACS Nano* **14,** 6165–6170 (2014).
13. D. S. Tsai *et al.* Few-Layer MoS_2 with High Broadband Photogain and Fast Optical Switching for Use in Harsh Environments. *ACS Nano* **7,** 3905–3911 (2013).
14. W. Zhang *et al.* High-Gain Phototransistors Based on a CVD MoS_2 Monolayer. *Adv. Mater*. **25,** 3456–3461 (2013).
15. W. Choi *et al.* High-Detectivity Multilayer MoS_2 Phototransistors with Spectral Response from Ultraviolet to Infrared. *Adv. Mater*. **24,** 5832–5836 (2012).
16. M. Buscema *et al.* Photocurrent generation with two-dimensional van der Waals semiconductors. *Chem. Soc. Rev*. **44,** 3691–3718 (2015).
17. M. Z. Hasan & C. L. Kane. Topological insulators. *Rev. Mod. Phys*. **82,** 3045–3067 (2010).
18. X.-L. Qi & S.-C. Zhang. Topological insulators and superconductors. *Rev. Mod. Phys*. **83,** 1057–1110 (2011).
19. L. He *et al.* Epitaxial growth of Bi_2Se_3 topological insulator thin films on Si (111). *J. Appl. Phys.* **109,** 103702-1–103702-6 (2011).
20. Q. Wang *et al.* Rational Design of Ultralarge $Pb_{1-x}Sn_xTe$ Nanoplates for Exploring Crystalline Symmetry-Protected Topological transport. *Adv. Mater.* **28,** 617–623 (2016).
21. A. Sharma *et al.* High performance broadband photodetector using fabricated nanowires of bismuth selenide. *Sci. Rep*. **6,** 19138–19145 (2016).
22. H. Zhang *et al.* Anomalous Photoelectric Effect of a Polycrystalline Topological Insulator Film. *Sci. Rep.* **4,** 5876–5880 (2014).
23. J. D. Yao *et al.* Ultra-broadband and high response of the Bi_2Te_3-Si heterojunction and its application as a photodetector at room temperature in harsh working environments. *Nanoscale* **7,** 12535–12541 (2015).
24. J. D. Yao *et al.* Layered-material WS_2/topological insulator Bi_2Te_3 heterostructure photodetector with ultrahigh responsivity in teh range from 370 to 1550 nm. *J. Mater. Chem. C* **4,** 7831–7840 (2016).
25. J. D. Yao *et al.* Ultra-broadband and high-responsive photodetectors based on bismuth film at room temperature. *Sci. Rep.* **5,** 12320–12326 (2015).
26. K. Zheng *et al.* Optoelectronic characteristics of a near infrared light photodetector based on a topological insulator Sb_2Te_3 film. *J. Mater. Chem. C* **3,** 9154–9160 (2015).
27. C. K. Lee *et al.* Robustness of a Topologically protected Surface state in a Sb_2Te_2Se single crystal. *Sci. Rep*. **6,** 36538 (2016).
28. S. M. Huang *et al.* Observation of surface oxidation resistant Shudnikov-de Haas oscillations in Sb_2SeTe_2 topological insulator. *J. Appl. Phys* **121,** 054311-1–054311-4 (2017).
29. W. C. Shen *et al.* Photoconductivities in MoS_2 Nanoflake Photoconductors. *Nanoscale Research Lett*. **11,** 124–130 (2016).
30. O. Lopez-Sanchez *et al.* Ultrasensitive photodetectors based on monolayer MoS_2. *Nat. Nanotech*. **8,** 497–501 (2013).
31. S. M. Huang *et al.* The linear megnatoresistance from surface state of the Sb_2SeTe_2 topological insulator. *J. Appl. Phys*. **119,** 245110-1–145110-4 (2016).
32. F. Gonzalez-Posada *et al.* Room-Temperature Photodetection Dynamics of Single GaN Nanowires. *Nano Lett*. **12,** 172–176 (2012).
33. J. D. Yao *et al.* Stable, Fast UV-Vis-NIR Photodetector with Excellent Responsivity, Detectivity, and Sensitivity Based on α-In_2Te_3 films with a Dirac band gap. *ACS Appl. Mater. Interface* **8,** 20872–20879 (2016).
34. H. Qiao *et al.* Broadband Photodetectors Based on Graphene-Bi_2Te_3 Heterostructure. *ACS Nano* **9,** 1886–1894 (2015).
35. C. Zang *et al.* Photoresponse properties of ultrathin Bi_2Se_3 nanosheets synthesized by hydrothermal intercalation and exfoliation route. *Appl. Surf. Sci.* **316,** 341–347 (2014).
36. D. H. Kang *et al.* High-Performance Transition Metal Dichalcogenide Photodetectors Enhanced by Self-Assembled Monolayer Doping. *Adv. Funct. Mater.* **25,** 4219–4227 (2015).
37. J. D. Yao *et al.* Stable, highly-respinsive and vroadband photodetection based on larger-area multilayered WS_2 films grown by pulsed-laser deposition. *Nanoscale* **7,** 14974–14981 (2015).
38. Z. Q. Zhang *et al.* Flexible, transparent and ultra-broadband photodetector based on large-area Wse_2 film for wearable devices. *Nanotechnology* **27,** 225501–225511 (2016).
39. W. J. Zhang *et al.* Role of Metal Conteacts in High-Performance Phototransistors Based on Wse_2 Monolayers. *ACS Nano* **8,** 8653–8661 (2014).
40. J. D. Yao, Z. Q. Zhang & G. W. Yang, Promoting the Performance of Layered-Material Photodetectors by Alloy Engineering. *ACS Appl. Mater. Interface* **8,** 12915–12924 (2016).
41. L. Yin *et al.* Ultrahigh Sensitive $MoTe_2$ phototransistors driven by carrier tunneling. Appl. Phys. Lett. **108,** 043503-1–043503-5 (2016).
42. L. Yin *et al.* Ultrafast and ultrasensitive phototransistors based on few-layered $HfSe_2$. Appl. Phys. Lett. **109,** *213105-1*-213105–5 (2016).
43. B. Robin *et al.* Extraordinary Photoresponse in Two-Dimensional In_2Se_3 Nanosheets. *ACS Nano* **8,** 514–521 (2014).
44. Z. Chen, J. Biscaras & A. Shukla, A high performance graphene/few-layer InSe photo-detector. *Nanoscale* **7,** 5981–5986 (2015).
45. Y. H. Huang *et al*. Electronic transport in $NbSe_2$ two-dimensional nanostructures: semiconducting characteristics and photoconductivity. *Nanoscale* **7,** 18964–18970 (2015).

Acknowledgements

The work was supported by the Taiwan National Science Council through Grants No. MOST 103-2112-M-110-009-MY3, NSYSU-KMU co-operation project No. 103-I 008. for SMH, and Grant No. MOST 105-2112-M-011-001-MY3 for RSC.

Author Contributions

S.M.H. conceived and designed the study, analyzed the data and wrote the manuscript. Y.J.Y., S.H.Y. and M.C. grew the single crystal. S.J.H., H.W.Y., Y.S.C., and R.S.C. prepared the samples and performed the photocurrent experiments. All authors contributed to discusssion and reviewed the manuscrit.

Additional Information

Competing Interests: The authors declare no competing financial interests.

How to cite this article: Huang, S.-M. *et al.* Extremely high-performance visible light photodetector in the Sb_2SeTe_2 nanoflake. *Sci. Rep.* **7**, 45413; doi: 10.1038/srep45413 (2017).

Publisher's note: Springer Nature remains neutral with regard to jurisdictional claims in published maps and institutional affiliations.